DEPARTAMENT OF
MATERIALS SCIENCE

MARTIM FRANCISCO PALMA MESTRE
BSc in Materials Science and Engineering

DISSIMILAR WELDING OF CoCrFeMnNi HIGH ENTROPY ALLOY TO 316 STAINLESS STEEL

MASTER IN MATERIALS ENGINEERING
NOVA University Lisbon
September, 2023

DEPARTAMENT OF
MATERIALS SCIENCE

DISSIMILAR WELDING OF CoCrFeMnNi HIGH ENTROPY ALLOY TO 316 STAINLESS STEEL

MARTIM FRANCISCO PALMA MESTRE

BSc in Materials Science and Engineering

Adviser: João Pedro Oliveira
Assistant Professor, NOVA University Lisbon

Co-advisers: Jiajia Shen
Doctoral Student, NOVA University Lisbon

Examination Committee:

Chair: Alexandre José da Costa Velhinho
Assistant Professor, NOVA University Lisbon

Rapporteurs: Ivan Rodolfo Pereira Garcia de Galvão
Associate Professor, Instituto Superior de Engenharia de Lisboa

Adviser: João Pedro Oliveira
Assistant Professor, NOVA University Lisbon

MASTER IN MATERIALS ENGINEERING

NOVA University Lisbon
September, 2023

Dissimilar welding of CoCrFeMnNi high entropy alloy to 316 stainless steel

ACKNOWLEDGMENTS

I would like to start by thanking my supervisors, Professor João Pedro Oliveira, and Doctoral student Jiajia Shen, for their expertise, guidance, and support throughout my research. Thank you for the challenges presented, as well as for the valuable feedback, during this year working on the dissertation. I would also like to thank the people in the Department of Mechanical and Industrial Engineering for always being available to help me improve my laboratory practices, as well as clarifying any questions or doubts I had.

Also, a special thank you to my family for always encouraging me to pursue a career in engineering and supporting me throughout these 5 years.

Finally, a huge thank you to my friends, who I know won't be reading this, but I want to leave in writing my full appreciation and gratitude for all the moments we shared in these 5 years.

Although few, I want all those whom I mentioned to know that these words are from the heart, and I really am grateful for all of you.

“Done is better than perfect.” (Sheryl Sandberg).

Motivation

Welding of high entropy alloys is a new field in material and mechanical engineering that has sparked interest due to the uniqueness of the materials involved. Unlike traditional alloys, high entropy alloys have a unique composition of multiple elements in almost equal proportions. This opens the door for a new set of qualities, such as extraordinary mechanical properties, high resistance to extreme temperatures, different types of corrosion and many others. Dissimilar welding is an already commonly used technique for joining different materials, and, consequently, their different and complementary properties. So, the basis of this work is using the principle of dissimilar welding and applying it to a high entropy alloy.

The selected high entropy alloy CoCrFeMnNi has already been used for similar research, however, it was joined to the other base material 316 Stainless steel through laser welding. The point behind the selected materials is to try and couple the excellent mechanical properties of the high entropy alloy with the corrosion resistance of the 316 stainless steel.

In this work, gas tungsten arc or TIG welding is the chosen technique. With this, the motivation behind this paper is to know how the welding technique impacts the microstructure, the phases formed, the mechanical properties, and assess if it has the potential to be applied in structural-oriented applications.

ABSTRACT

High entropy alloys have gathered recent attention due to their extraordinary mechanical properties. And with that comes the desire to couple those properties with others from different materials, through dissimilar welding. In this work, gas tungsten arc welding is used to fuse together a CoCrFeMnNi high entropy alloy to a commercially available 316 stainless steel. The objective is to try to add the former's high fracture toughness and ductility to the latter's excellent corrosion resistance and see if it can be employed in structural-oriented applications. Two different samples were made to compare the influence of post-weld heat treatments on the microstructure and mechanical properties. The microstructure study and evaluation were done resorting to optical and electron microscopy and X-ray diffraction. The mechanical properties were determined using a microdurometer and tensile testing. The microstructure was then assessed and correlated with the results of the mechanical tests. The results show a significant difference in hardness throughout the welded joints. The as-rolled sample shows a decrease of about 200 HV between the CoCrFeMnNi and the 316 stainless steel with a hardness value of about 150 HV in the fusion zone. The as-annealed sample maintains a constant HV value throughout the welded joint, of around 160 to 170 HV. This is coherent with the electron microscopy observations and may be a result of a new solid solution forming in the fusion zone. The tensile tests show both samples fractured at the fusion zone. This difference in ductility and hardness can be explained by the increase in grain size and stress relief from the annealing.

Keywords: High Entropy Alloy, Stainless Steel, Dissimilar Welding, Gas Tungsten Arc Welding, Annealing, Mechanical Properties, Microstructure.

RESUMO

Recentemente, as ligas de alta entropia têm recebido atenção devido às suas extraordinárias propriedades mecânicas. E com isso, surge o desejo de associar essas propriedades a outras de materiais diferentes, através de soldadura dissimilar. Neste trabalho, utilizou-se soldadura TIG para juntar uma liga de alta entropia CoCrFeMnNi a um aço inoxidável 316, disponível no mercado. Teve-se como objetivo juntar a elevada resistência à fratura e ductilidade da primeira à excelente resistência à corrosão do segundo, e ver se há potencial para serem utilizados em aplicações estruturais. Foram realizadas duas amostras diferentes para comparar a influência do tratamento térmico pós-soldadura na microestrutura e nas propriedades mecânicas. Os estudos da microestrutura foram feitos recorrendo a microscopia ótica e eletrónica e a difração de raios-x. As propriedades mecânicas foram determinadas com recurso a um microdurómetro e a ensaios de tração. A microestrutura foi então avaliada e correlacionada com os resultados dos ensaios mecânicos. Os resultados mostram uma diferença significativa de dureza ao longo das juntas. A amostra sem tratamento térmico mostra uma redução de cerca de 200 HV entre a parte CoCrFeMnNi e o aço inoxidável 316, com um valor de dureza de cerca de 150 HV na zona de fusão. Enquanto a amostra recozida mantém um valor de HV constante ao longo de toda a junta, de cerca de 160 a 170 HV. Os resultados são coerentes com as observações de microscopia eletrónica, e podem ser o resultado da formação de uma nova solução sólida na zona de fusão. Os ensaios de tração mostram ambas as amostras a fraturarem na zona de fusão. Esta diferença de ductilidade e dureza pode ser explicada pelo aumento no tamanho de grão e pelo alívio de tensões resultante do recozimento.

Palavras-chave: Ligas de Alta Entropia, Aço Inoxidável, Soldadura Dissimilar, Soldadura TIG, Recozimento, Propriedades Mecânicas, Microestrutura.

CONTENTS

LIST OF FIGURES

LIST OF TABLES

ACRONYMS

AC	Alternating current
DC	Direct current
FCC	Face-centered cubic
FZ	Fusion zone
HAZ	Heat-affected zone
HEA	High entropy alloy
PWHT	Post-weld heat treatment
SEM	Scanning electron microscope
SS	Stainless steel
TIG	Tungsten inert gas
XRD	X-ray diffraction

SYMBOLS

F	Number of degrees of freedom
C	Number of components
P	Number of phases
σ_u	Ultimate strength
σ_y	Yield strength
ε_f	Fracture strain

1

INTRODUCTION

High entropy alloys (HEAs) are a new class of materials that have gathered recent attention due to their unique properties. Depending on the elements present in its constitution, this type of alloy can have extraordinary functional features. So, the driving force behind the research on dissimilar welding of HEAs is the desire to combine their properties with others from other materials in a single welded joint. Recent research on dissimilar welding mainly focuses on the evaluation of the weld integrity with non-destructive testing methods, and the development of new models and simulations that can accurately predict the weld's properties [1].

However, the formation of damaging phases may occur when two base materials are welded simultaneously. This depends on the constitution of the materials employed, the consequential mix of elements on the fusion zone (FZ), as well as the thermal cycle experienced. So, to fully optimize and utilize the full benefits of HEAs, it is crucial to study the microstructure evolution pre- and post-heat treatment of dissimilar welded joints.

Different welding techniques have been used on the HEA CoCrFeMnNi such as friction stir welding [2] or electron beam welding [3], with the results demonstrating that the alloy presents good weldability. But most of this work has been with similar welding, whereas dissimilar welding research of a HEA hasn't had as much focus.

1.1 Dissimilar welding

Fusion welding is a fabrication process that consists of joining two separate materials, mainly of metal origin, by fusing them. It uses electricity to create an arc between an electrode, causing the metal to heat up and, eventually, melt and fuse with another material. There is a plethora of welding techniques used in the manufacturing industry. However, dissimilar welding is becoming more and more prevalent due to its ability to couple the different properties of the materials involved, thus bringing a new set of quality properties to the base material. This means that the welding of dissimilar metals has unmeasured potential to play a fundamental role in increasing the functionality of structural components, for example. Dissimilar welding involves joining two or more different types of metals or alloys. It's used in a variety of applications, including pressure vessels and structural steel components, as well as, in the restoration of damaged metal components. It can be difficult to achieve a properly welded dissimilar joint since the different components may have conflicting physical and mechanical properties, such as different melting points, thermal expansion coefficients or thermal conductivities. Appropriate filler material, special techniques, and proper equipment are required to overcome these difficulties. Its optimization remains a big topic for researchers. Even so, dissimilar welding is effective in reducing manufacturing costs and time reducing, especially in the automotive industry [4].

1.2 High entropy alloys

Most alloys used in the manufacturing industry are made from one or two base elements, with a variety of others present in negligible percentages. In contrast, HEAs include five or more elements in about equal amounts and have a high degree of disorder [5]. This results in a high number of possible arrangements of different elements to suit different needs. These compositions, however, are mostly discovered through trial and error, with only a few being proven useful. Not only that but the exact alloy composition, as well as other variables such as the welding technique and the materials' microstructural properties, affect the weldability of HEAs and their future use [6].

Multiple phases that make up their microstructures are what distinguish them from conventional alloys and can result in special mechanical qualities. There have been reports of HEAs with fracture toughness superior to those of pure metals, and high resistance to corrosion and oxidation [7], [8].

According to Yeh et al. [9] the reasons HEAs demonstrate these unique properties are mainly due to four effects: the high entropy effect, related to the inherent entropy of the system configuration, makes it easier to form solid solution phases by lowering their free energy; the sluggish diffusion effect, where the elements with a higher configurational entropy of mixing have a slower diffusion when compared to those with a lower configurational entropy. This leads to the formation of nano precipitates; the severe lattice distortion effect, caused by the discrepancy in atom size between the different alloy components, is responsible for the slow kinetics in HEAs; the cocktail effect, where adding specific elements may enhance certain properties of the alloys.

1.3 Materials

1.3.1 CoCrFeMnNi

The CoCrFeMnNi HEA, also known as a Cantor alloy, is a solid-state solution alloy, named after its discoverer Brian Cantor *CBE FREng*. As reported by Cantor in its 2004 paper [10], an alloy was made compromised of 20 elements at 5 at%, namely Ag, Al, Bi, Cd, Co, Cr, Cu, Fe, Ge, Mg, Mn, Mo, Nb, Ni, Pb, Sb, Si, Sn, W, Zn. According to Gibbs' phase rule (1), at constant pressure, up to 21 distinct phases could form at equilibrium, but, as results show, significantly fewer phases formed. Due to the systems' high configurational entropy, a single face-centered cubic (FCC) solid-solution phase was the resulting predominant phase, mainly composed of Co, Cr, Fe, Mn, and Ni. Thus, creating the Cantor HEA.

$$F = C - P + 2 \tag{1}$$

This HEA sparks interest due to bending the Hume-Rothery rules, that state that both solvent and solute elements must have the same crystal structure to form a solid solution. In the CoCrFeMnNi alloy, in equimolar concentration, there is no noticeable distinction between solute and solvent elements, while as pure elements all have different crystal structures [11]. It is considered in the literature as a model alloy, because, independently of the exact composition, it maintains a single phase with FCC structure. This has been reported with $Co_5Cr_2Fe_{40}Mn_{27}Ni_{26}$ [12] and $CoCrFeMn_{0.5}Ni$ [13]. And changing the composition may be a way to improve both the mechanical properties and the FCC single-phase stability, according to Yao et al [12].

In its equiatomic form, the CoCrFeMnNi HEA is well recognized for exhibiting outstanding mechanical qualities even at extremely low temperatures, such as 77K, the liquid nitrogen temperature [7]. This includes high fracture toughness, high-temperature structural stability, excellent ductility as well as strong corrosion resistance, but a low enough yield strength that prevents it from being used in structural applications.

Table 1 - CoCrFeMnNi properties, retrieved from [14]–[17]

Property	Value	Unit
Tensile Strength	427	MPa
Yield Strength	194	MPa
Fracture Strain	92	%
Microhardness	~425	HV
Young Modulus	~177	GPa
Thermal Conductivity	13.5	W/(m.K)
Melting Point	~1550	K

Due to the elements' high melting temperatures and propensity to create brittle, hard intermetallic phases, cobalt-based alloys can often be difficult to weld. So, to prevent faults from forming and to guarantee the integrity of the weld, it's crucial to carefully select both the welding technique as well as the other base material used in dissimilar welding.

1.3.2 316 stainless steel

A famous choice for a base material for its high strength and durability. With high yield and tensile strength make it suitable for use in structural applications. Due to its higher tensile strength and heat resistance than mild steel, 316 stainless steel (SS), despite being a good welding option, is generally more challenging to weld. To stop hard, brittle martensite from forming in the welded area, it's critical to utilize a low-hydrogen welding method and maintain a low heat input. For the welded area to prevent cracking, its also crucial to pay attention to the cooling rate [18], [19].

The 316 nomenclature comes from the molybdenum and chromium percentages, 3% Mb and 16% Cr. These elements, as well as the high percentage of Ni, make it more corrosion-resistant than other varieties of SS. Despite being resistant to general corrosion, local forms of corrosion attacks, like pitting corrosion, are prevalent in 316 SS. This situation can be avoided by increasing the percentages of molybdenum and chromium [20].

1.4 Materials and processing methods

1.4.1 TIG welding

TIG is regarded as the preferred method for fusing metals that are, in theory, not compatible. When welding in such conditions, more attention must be taken to the electrode composition, welding process, etc. TIG stands for *Tungsten Inert Gas,* referring to the tungsten electrode and inert atmosphere required for this technique. The atmosphere can be achieved with Argon (Ar), Helium (He), or a mixture of both, and the technique consists of maintaining an arc in an inert environment between the electrode and the workpiece. With TIG is possible to raise the weld depth/width ratio and decrease the heat-affected zone (HAZ) range at will, thus producing weld deposits of great quality with substantially reduced equipment costs [21].

To preserve the integrity of the welded joint and of the tungsten electrode, preventing it to overheat and burn, is advised to use straight polarity with alternating current (AC). With an AC, the heat input to the tungsten electrode is averaged out as the wave moves from one side to the other. But, due to the low thermal conductivity and a higher thermal expansion coefficient of SS compared to those of ferritic steels, a direct current (DC) is favored [21]. When applied in HEAs, the joints produced are of high performance and defect-free, as demonstrated by recent research [22]. Although, the quality of joints made from HEAs depends on what elements are present in its constitution.

1.4.2 Post-weld heat treatment

Post-weld heat treatments (PWHT) have the purpose to alleviate any residual stresses and improve the mechanical properties of the materials subjected to such treatments. It involves heating and cooling a metal or alloy and can be different processes. The one employed on this welded joint is called annealing. This heat treatment has the objective of softening the metal, making it more malleable, by increasing the ductility and reducing the hardness. By heating the metal to a temperature below its melting point, and then letting it slowly cool, due to phase recrystallization the grain size is refined, and internal stresses are relieved, thus improving ductility [23].

More specifically, when HEAs are annealed their properties are enhanced as reported by Tsai et al. [24]. But, regarding the HEA CoCrFeMnNi, annealing temperatures between 650ºC and 800ºC show very little increase in grain size and so no changes in the mechanical properties. This HEA shows a high recrystallization temperature, so adequate annealing should be with temperatures superior to 900ºC [25].

1.5 State of the art

Research on CoCrFeMnNi welding mainly focuses on similar welding [17], [26]. It has been established that whether the welding technique is laser or TIG that the HEA has good weldability. Research from Oliveira et al. [17] investigated what effects TIG welding had on the CoCrFeMnNi HEA. The results showed no welding defects, proving that the CoCrFeMnNi is suitable for TIG welding. When analyzing the post-weld HEAs' microhardness, in the FZ, the hardness was like what is found in an as-cast HEA. But, in the HAZ, the grain size altered, due to the thermal cycle experienced, which was reflected in the microhardness testing. The large grain size and poor hardness of the FZ, which encourage larger strain accumulation in this area, resulted in a drop in the joint fracture strain. Additionally, after welding, the ductility of the joints was reported to be lower than that of the base material.

Dissimilar welding of CoCrFeMnNi, however, needs more research to make sure it can have a future in structural applications. Oliveira et al. [27] worked on laser welding of CoCrFeMnNi to a 316 SS. The difference regarding other arc-based welding processes, like TIG, is in the size of FZ, where there is more room for the grain to grow, and, consequently, different mechanical properties. With a more reduced and concentrated heat source, laser welding also reduces the size of the HAZ, a significant weak point of welded joints. It was reported a hardness increase in the FZ, which was attributed to the incorporation of the carbon from the 316 SS and a solid solution strengthening, as a result of the mixture of base materials.

2

MATERIALS AND METHODS

This project planned the fabrication of a dissimilar welded joint with a CoCrFeMnNi HEA and a commercially available 316 stainless steel as base materials. Two different samples were made. One underwent a PWHT for 1 hour at 1000ºC and the other remained in the as-rolled. The welding technique selected was TIG welding. For the microstructure characterization, the techniques used for both samples were optical (OM) and electron microscopy (SEM) and X-ray diffraction (XRD). For the mechanical characterization, microhardness and tensile testing was performed.

2.1 Sample Preparation

Before welding, the base materials underwent a cleaning process with alcohol and acetone to remove any impurities. The sheets of the base materials were butt joined using TIG welding. The resulting as-rolled welded joint had a length of 65 mm, a width of 30 mm and a thickness of 1,54 mm. For the as-annealed joint, 3 samples were achieved with lengths of 65 mm and 75 mm, an equal width of 30 mm and a thickness of 1,57 mm. Both samples are depicted in Figure 2.1.
For an easier analysis and characterization, the samples were cut into dog-bone shapes, as demonstrated with Figure 2.2.

a) b)

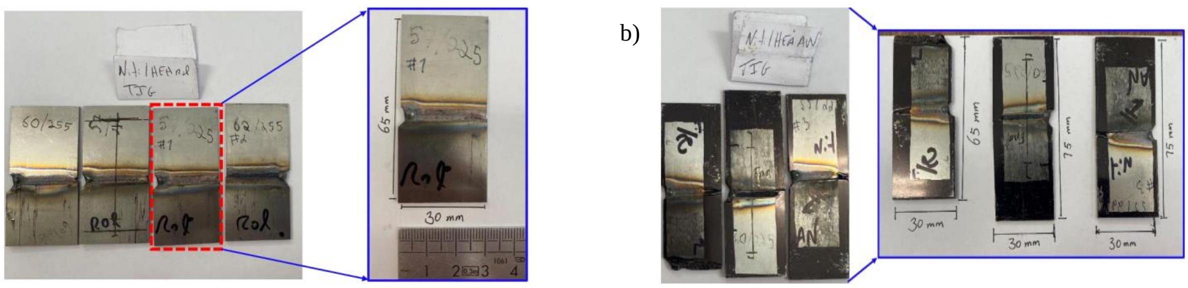

Figure 2.1. (a) As-rolled welded joint; (b) As-annealed welded joint

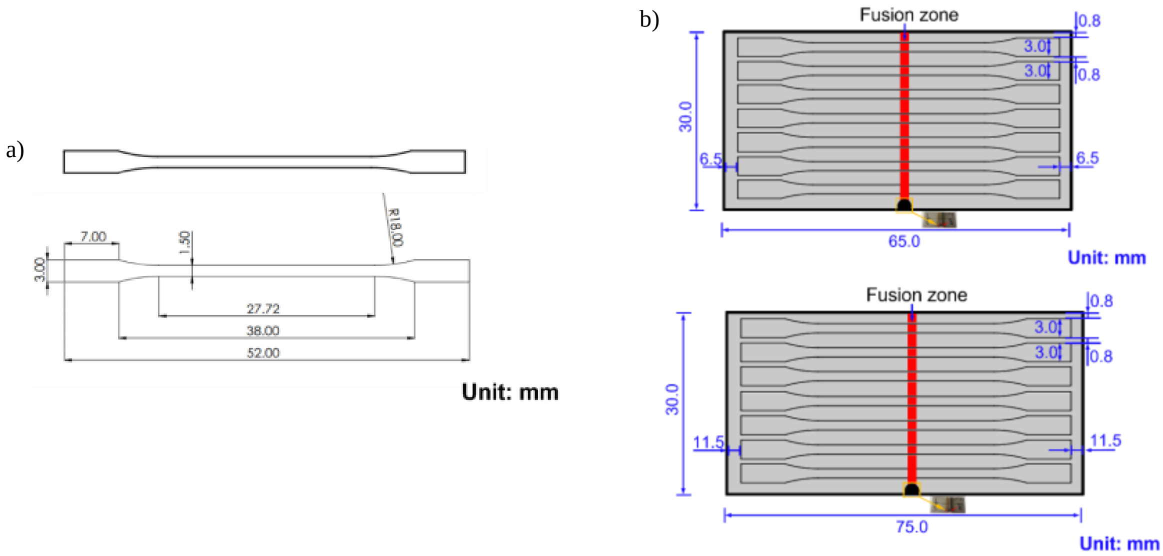

Figure 2.2. (a) Dog-bone dimensions for the as-rolled and as-annealed samples; (b) Sheet and dog-bone dimensions for the as-rolled and as-annealed samples

After the cutting was complete, the samples were polished in a MECATECH 335-PRESI with sandpaper starting from P240 gradually increasing all the way to P4000. To finalize the process, after the P4000, the samples were polished with diamond paste until a mirror-like surface was obtained. To bring out the microstructure, the samples were etched using a solution of HCl and HNO_3. A Leica DMI5000M OM was simultaneously used to make sure that the grains were visible across all the welded joints.

2.2 Characterization

SEM observations were done with a JEOL JSM 7000, with the objective of evaluating the microstructure evolution across the welded joints. To complement SEM analysis, high energy synchrotron XRD was performed to discover which phases formed across the whole sample, with special attention on the FZ and HAZ.

For the Vickers microhardness measurements, it was used a ZHV1-m hardness testing machine. It was applied a load of 0,5 kgf with an indentation time of 10s. 6 lines total along the transversal section with 100μm between each indentation, both vertically and horizontally, as schematized in Figure 2.3. To determine the ductility and strength of the joints, tensile testing was performed until failure, with a Shimadzu AG-50kNG machine.

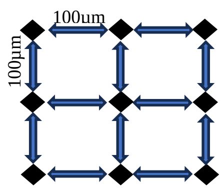

Figure 2.3 - Hardness measurements schematic

3

RESULTS AND DISCUSSION

3.1 OM + SEM

Figure 3.1 shows an overview of the as-rolled dissimilar welded joint. Full penetration was obtained, with no welding defects detected and a wide FZ, resulting from the less controlled heat input of TIG, when compared to laser welding [27]. The unevenness of dark tones can be attributed to an over-etching of some regions resulting from non-homogeneous mixing of the two base materials, enhancing some of the microstructure at particular regions.

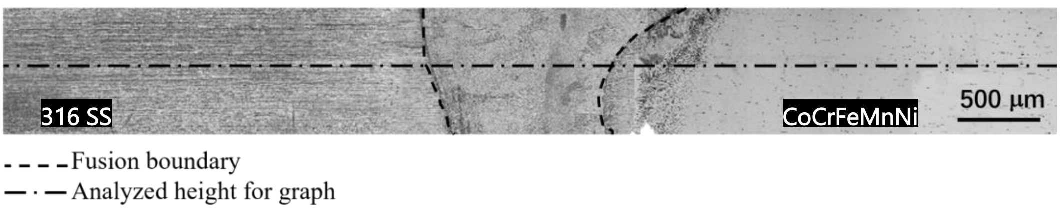

Figure 3.1 - As-rolled welded joint overview, obtained by OM.

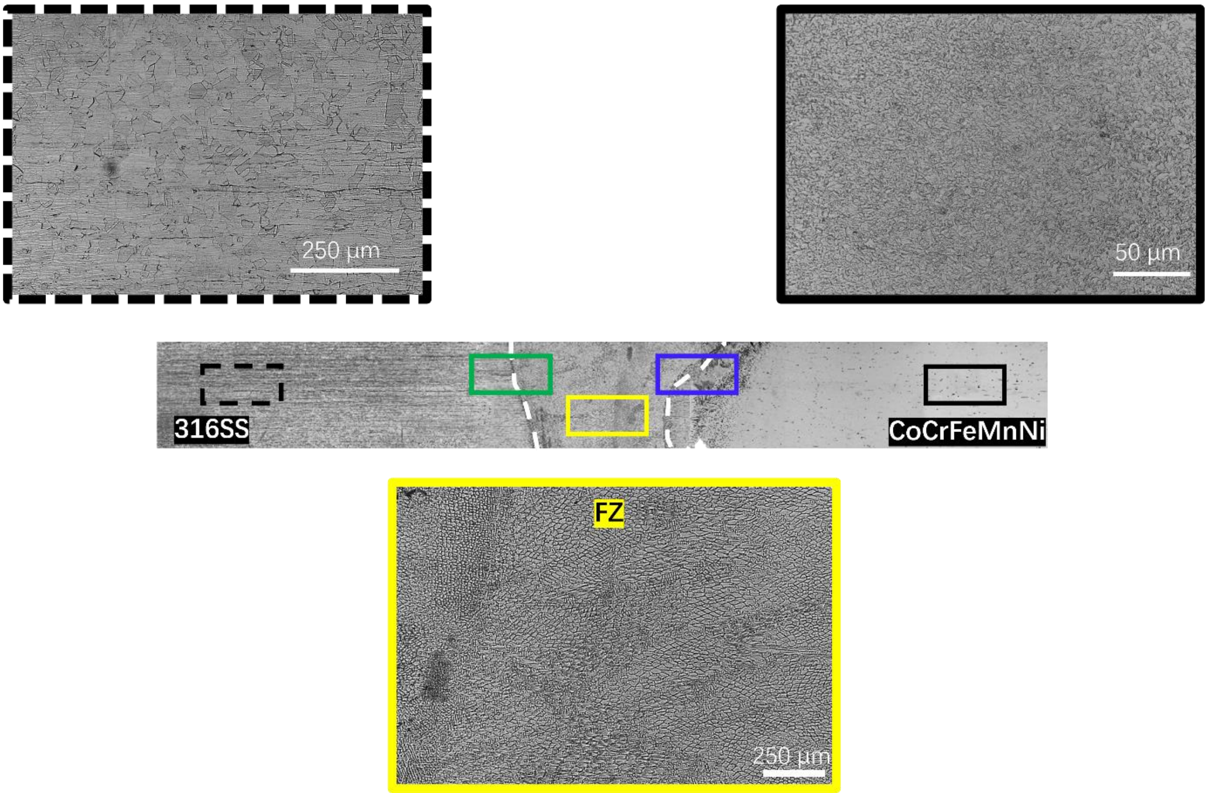

Figure 3.2 - FZ and base material microstructures of the as-rolled welded joint, obtained by SEM.

As Figure 3.2 depicts, the different microstructures can be easily noticed in the regions of the as-rolled joint. The CoCrFeMnNi base material presents a fine grain with a pancake-liked shape, with a heterogenous distribution of grain size. As it nears the FZ, the grain size increases, because of the heat diffusion, causing it to recrystallize and grow. The heat input on TIG is less precise, leading to a larger HAZ, as opposed to other welding techniques such as laser welding.

In this region, as demonstrated with Figure 3.3a, a dendritic microstructure is formed. In the FZ, we observe the biggest grain size across the whole joint. The weld centerline is the region that experienced the peak temperature of the welding process, thus leading to the grains closest to the interface to solidify first and not growing as much, when compared to those at the center of the FZ. These grains are finer and with an equiaxial shape, whereas the FZ grains are large and columnar. The grain size and shape remain constant until reaching the boundary of the FZ with the 316 SS base material. Here, unlike the FZ boundary with the CoCrFeMnNi, dendrites didn't form. Both the 316 SS base material and HAZ show an austenitic microstructure, with an equiaxial grain shape, as shown with Figure 3.2 and 3.3b, respectively, with a minor grain refinement in the HAZ. This can be explained by the difference in thermophysical properties between the two base materials. The 316 SS possesses a good heat resistance, leading it to not being majorly influenced by the heat input, and thus preserving its grain size throughout the HAZ and base material.

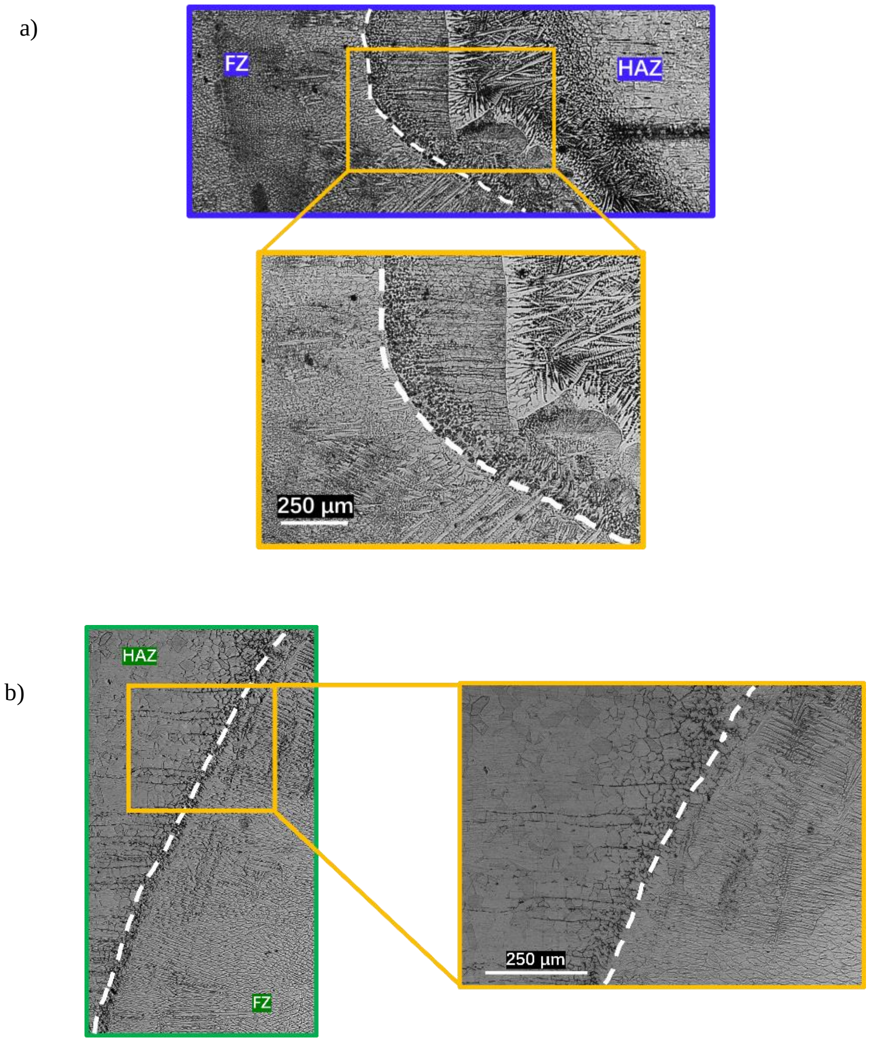

Figure 3.3. (a) HAZ and FZ microstructure of the CoCrFeMnNi side of the welded joint, obtained by SEM; (b) FZ and HAZ microstructure of the 316 Stainless steel side of the welded joint, obtained by SEM.

Figure 3.4 shows an overview of the as-annealed welded joint, obtained by OM. In this sample, similar to the as-rolled, full penetration was obtained with no welding defects and FZ close in size. The etching was uniform throughout the whole sample.

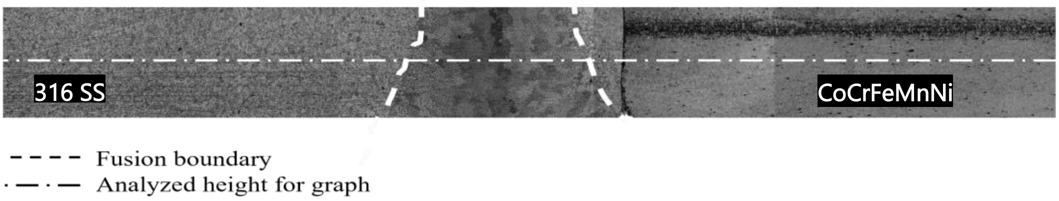

Figure 3.4 - As-annealed welded joint overview, obtained by OM.

As observed in Figure 3.5, after the heat treatment, the grain size increased throughout the welded joint, but maintaining an almost constant size, meaning the annealing served its purpose. Although, it is noticeable a subtle difference in grain shape and size, between both base materials. In Figure 3.5, the microstructure of the CoCrFeMnNi has a finer and pancake-shaped grain, whereas the 316 SS presents a bigger grain with an equiaxial shape with sharper boundaries. In the HAZ of the HEA side it is observed a slight increase in grain size, as a result of the thermal cycle experienced, and a disappearance of the dendrites previously present in the as-rolled joint. A possibility is that the recrystallization and high annealing temperature helped forming new grains and promoting the diffusion of atoms, which helped breaking up the dendritic structures [28]. For the HAZ of the 316 SS, no change in size or grain shape was noticeable, however, it shows an appearance of annealing twins. These are commonly formed during the recrystallisation of cubic structural metals, such as both base materials in study, as a consequence of growth accidents, mainly, the stacking of the [111] planes [29].

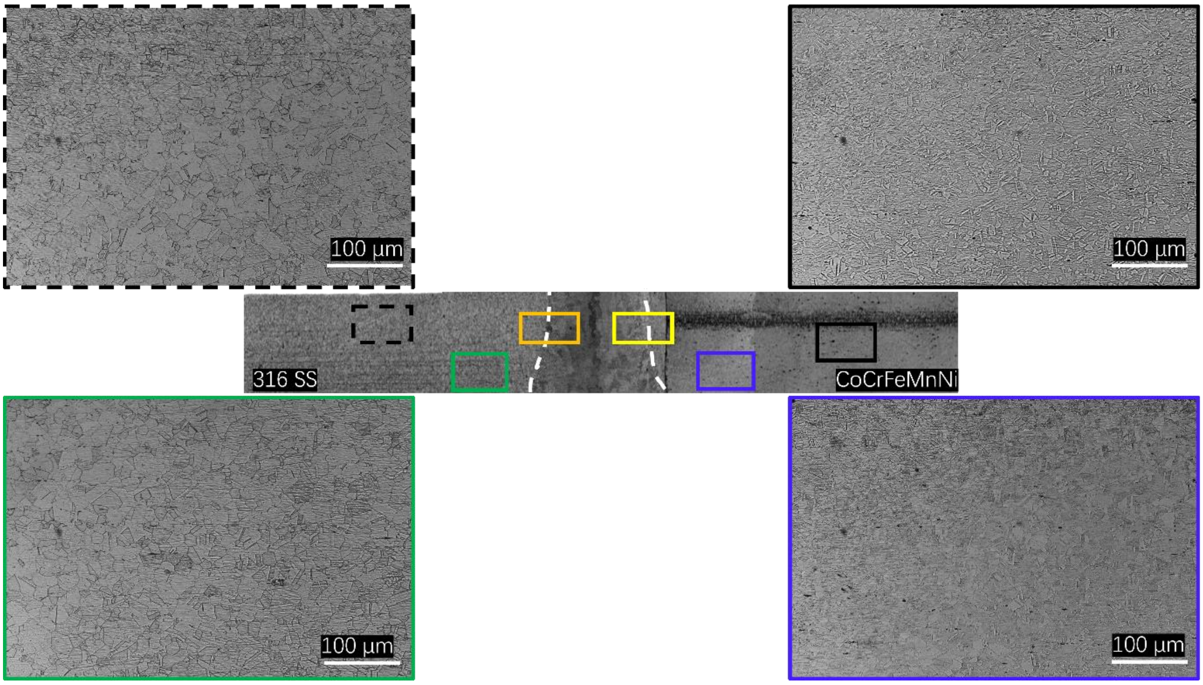

Figure 3.5 - Base materials and HAZs microstructures of the as-annealed welded joint, obtained by SEM.

The FZ shown in Figure 3.6a and 3.6b show a different microstructure when compared to that of the as-rolled joint. Here a few dendrites can be observed the closer it gets to the weld centerline. Near both boundaries, these dendrites become less frequent, and recrystallization occurs, leading to the formation of small equiaxial grains.

a)

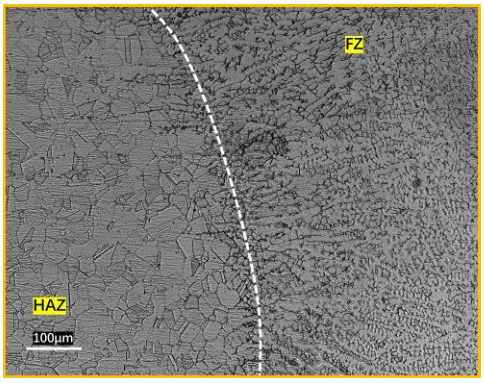

b)

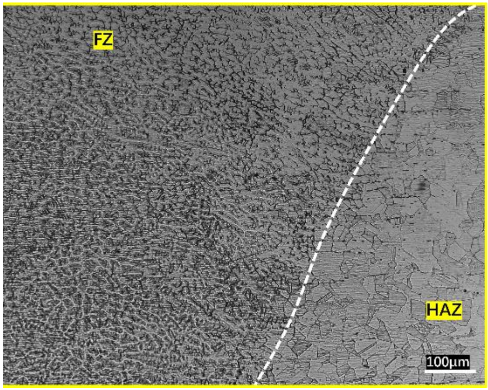

Figure 3.6. (a) HAZ and FZ microstructure of the 316 Stainless steel side of the as-annealed welded joint, obtained by SEM; (b) FZ and HAZ microstructure of the CoCrFeMnNi side of the as-annealed welded joint, obtained by SEM.

3.2 XRD

To identify the existing phases across the welded joints, high energy synchrotron XRD was performed. The diffraction patterns of the as-rolled welded joint are depicted in Figure 3.7.

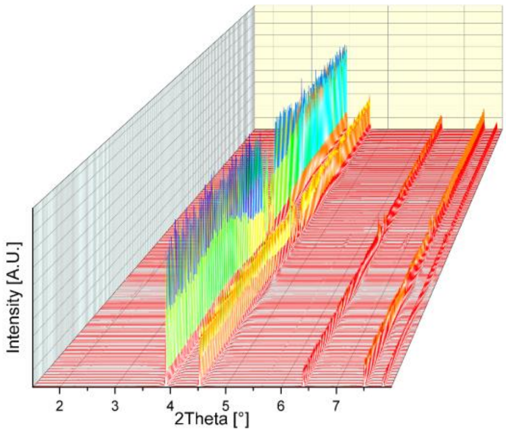

Figure 3.7 - As-rolled XRD patterns

It is known from previous studies that the HEA CoCrFeMnNi has a FCC structure, but small inclusions from oxides or other contaminations can appear and slightly alter the structure. All peaks indexed are of FCC structure. The first and most intense peak at $2\theta \approx 4^{o}$ corresponds to a FCC [111] in the HEA and for the γ phase, or austenite, in the 316 SS, as reported by Peng et al. [30] and Mahdi et al. [31], respectively. Which means that the more abundant phases are of FCC [111] crystallographic structure, as expected, as both base materials individually have a FCC structure. At the same 2θ value a small peak is detected from the α phase, or ferrite, with a BCC [110] crystalline structure. The appearance of α-ferrite can be explained by the relatively slow cooling rate from the γ-austenite phase. The γ phase can also be identified in the rest of the peaks with [200], [220], [331] and [222] crystal structures.

The diffraction patterns for the as-annealed welded joint are illustrated in Figure 3.8.

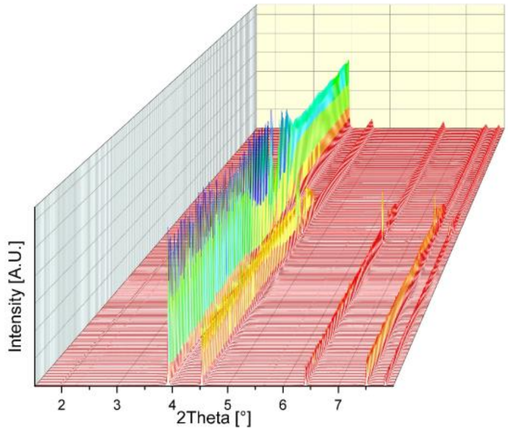

Figure 3.8 - As-annealed XRD patterns

No noticeable difference in the diffraction patterns was detected when compared to those of the as-rolled. A possible explanation for this can be that the PWHT did not influence the crystalline structure or the orientation of both base materials, maintaining its original texture despite changing the grain size.

3.3 Hardness

The Vickers microhardness mapping results are displayed in Figure 3.9. The HV values are in agreement with the results of the SEM. The CoCrFeMnNi presents a fine grain, translating it to a high HV value (≈ 425 HV), whereas the 316 SS has a lower HV (≈ 175HV), due to its larger grains. Both are coherent with the respective theoretical hardness values, but it is important to note that these values are not 100% constant, because different elements percentages in the alloys influence the final value [32], [33].

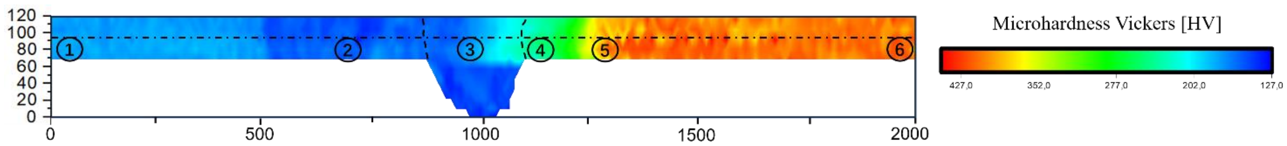

Figure 3.9 - As-rolled microhardness mapping

From Figure 3.9 and Figure 3.10, six different zones can be identified. The regions 1 and 2 correspond to the base material 316 stainless steel and its HAZ, respectively. The hardness value stays almost constant at 180 HV, up until reaching the FZ, where a slight decrease in HV value is noticed. At the FZ, region 3, the hardness reaches its lowest value of about 150 HV at mid-height, and of 127 HV in the whole FZ. Larger grains translate to less grain boundaries, and thus less obstacles for moving dislocations. It should also be noted that, in the FZ, the grains depicted by SEM are of columnar shape which have been reported to have more plasticity but less strength when compared to those of a more equiaxial shape [34]. Regions 4 and 5 represent the HAZ of the CoCrFeMnNi base material. Here the hardness goes through a sudden increase, which can be attributed to recrystallization and newly formed grains, as well as a decrease in grain size. At region 6, the hardness value of the CoCrFeMnNi base material stabilizes, reaching its highest value, as expected.

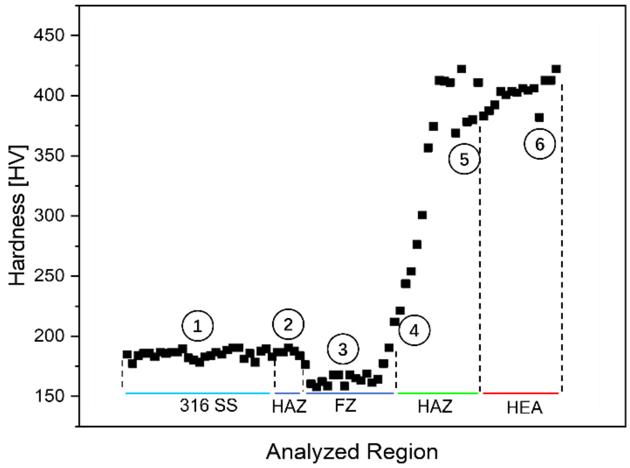

Figure 3.10 - As-rolled microhardness evolution at mid-height

The difference in HAZ sizes may be explained by the thermal properties of the base materials and the relation between grain size and thermal diffusivity. According to a report by Vilémová et al. [35] the presence of Mn in the HEA negates the contribution of the other elements with high thermal conductivity (Fe, Co etc.), and brings the thermal conductivity value of the alloy to about 13,5 W/mK at room temperature. A significantly lower value than that predicted by the rule of mixture, of about 75 W/mK. By having a low thermal conductivity, the heat inputted in the welding process accumulates near the FZ, leading to a growth of grain size across a larger area of the base material. Another possible explanation is that the small grain size the HEA presents in an as-cast state, the phonons aren't able to scatter, due to the high number of grains boundaries, thus reducing the thermal conductivity [36]. The same cannot be said about the HAZ of the 316 SS. While both have a relatively low thermal conductivity (16 W/mK for 316 SS), the grains of the 316 SS are bigger, which facilitates the heat diffusion, and so, the grain size is not as affected by it, preserving the hardness value.

Figure 3.11 and Figure 3.12 shows the hardness mapping of the welded joint PWHT. It is immediately noticeable that the hardness stabilized throughout the sample at ≈175 HV. A small increase to ≈ 200 HV is detected near the boundary between the FZ and the HAZ of the CoCrFeMnNi base material as well as a decrease to below average hardness in the same side. Similar results have been reported [37], where the HV values of a CoCrFeMnNi sample abruptly decreased for higher annealing temperatures, as a consequence of the start of recrystallization phenomena and grain growth. But for annealing temperatures below the recrystallization temperature, a slight increase in hardness is detected.

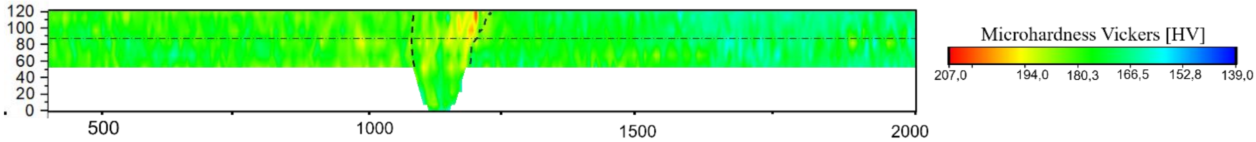

Figure 3.11 - As-annealed microhardness mapping

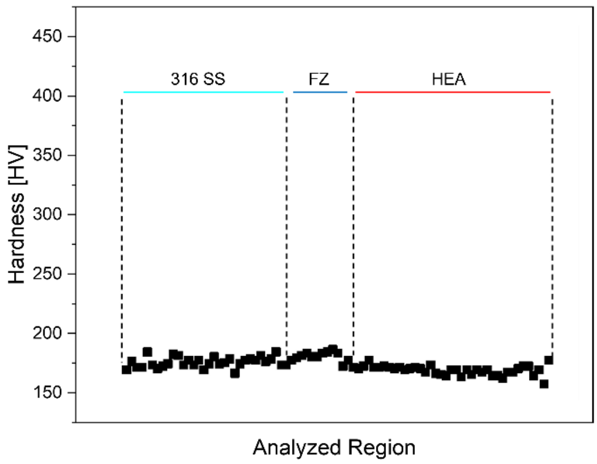

Figure 3.12 - As-annealed microhardness evolution at mid-height

3.4 Tensile tests

Tensile tests are a proper way to determine the mechanical properties of the joints, and, consequently, assess their suitability for structural applications. The mechanical properties of the individual as-cast and as-rolled base materials are shown in Table 1 and Table 2, respectively. These values are retrieved from the bibliography [27], [38], [39].

Table 2 - Mechanical properties of the as-cast base materials

Reference	Ultimate tensile strength [MPa]	Yield strength [MPa]	Fracture strain [%]
316 SS	580	290	50
CoCrFeMnNi	427	194	92

Table 3 - Mechanical properties of the as-rolled base materials

Reference	Ultimate tensile strength [MPa]	Yield strength [MPa]	Fracture strain [%]
316 SS	431	223	56.8
CoCrFeMnNi	943	587	9.5

When comparing the mechanical properties between the two states of the base materials, a clear difference is noted. For the 316SS base material, a significant decrease in both ultimate and yield strength occurs, while simultaneously a slight increase in fracture strain. And for the CoCrFeMnNi base material, the opposite happens. A significant increase in both ultimate and yield strength, and a decrease of fracture strain to about 10% of the as-cast value. Following this train of thought, additional treatment on the base materials, namely TIG welding and annealing, bigger changes in the mechanical properties are expected. As already evidenced, TIG welding caused significantly larger HAZs in the as-rolled welded joint than those of dissimilar laser welding [27]. This means that the microstructure is more heterogeneous, leading it to a complex mechanical response.

The stress/strain curves of the welded joints are represented in Figure 3.13. A summary of the mechanical properties calculated from the tensile tests are depicted in Table 3. The tensile testing occurred at a speed of 0,02 mm/s for both samples.

Both samples suffered the fracture at the fusion zone. The columnar microstructure at the as-rolled FZ helped form continuous pathways that enable crack propagation, facilitating the fracture. Whereas the dendritic microstructure at the as-annealed FZ results in non-uniform residual stresses distribution, contributing to crack formation and propagation.

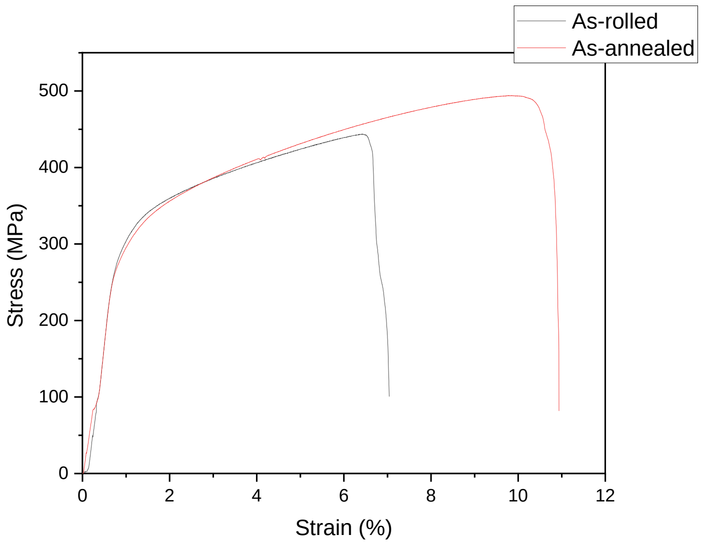

Figure 3.13 - Stress/strain curve of the welded joints

Table 4 - Mechanical properties of the as-rolled and as-annealed samples

Reference	Ultimate strength [MPa]	Yield Strength [MPa]	Fracture strain [%]
As-rolled sample	443	281	6.43
As-annealed sample	494	260	10.24

By comparing the samples, it is noticeable the influence of the heat treatment. The as-annealed sample displays a decreased in yield strength (σ_y = 281 MPa vs σ_y = 260 MPa), but an increase in both ultimate strength (σ_u = 443 MPa vs σ_u = 494 MPa) and fracture strain (ε_f = 6.43 vs ε_f = 10.24%). Meaning, the as-annealed lost about 20MPa of yield strength but became more ductile and capable of withstanding a higher load. These results are coherent with the microstructure observed by SEM. After the heat treatment, a more homogenous microstructure was obtained and accompanied by a stress relief. This directly contributed to an improvement of the mechanical properties. Even though the as-rolled welded joint is an overall worse performing joint, it still possesses good enough mechanical qualities to be applied in structural applications.

When the as-rolled joint is directly compared to one welded through laser welding [27], it shows that TIG welding produced a joint with inferior yield and ultimate strength, but more ductile. This may be explained by the fact that the heat input of TIG welding is less controlled, resulting in larger HAZs and, consequently, bigger microstructural changes. Thus, becoming less likely to retain the desired mechanical properties of the base materials.

Looking into the values presented in Table 1 and Table 2, the individual base materials have better mechanical properties. However, both joints show that when these materials are coupled, the extraordinary mechanical properties of each are mostly preserved, and new characteristics are gained, such as corrosion resistance.

4

CONCLUSIONS

Two welded joints composed of a CoCrFeMnNi high entropy alloy and 316 stainless steel were successfully obtained by TIG welding. No defects or pores were detected, with both base materials showing good weldability. By employing scanning electron microscopy, X-ray diffraction, hardness mapping and tensile testing it was possible to assess the mechanical properties of the welded joints and correlate them with the respective microstructures.

After the heat treatment, a more homogenous microstructure was obtained but the differences in grain shape between the two base materials were still noticeable. Additionally, the hardness values stabilized, with the difference between the highest and lowest point being of ≈ 60HV. In both samples, dendrites were obtained as a result of fast cooling. The welded joints in both conditions, as-rolled and as-annealed, presented good mechanical properties. The as-rolled showed an ultimate strength of ≈ 433 MPa, a yield strength of ≈ 281 MPa, and a fracture strain of ≈ 6.43%. Whereas the as-annealed showed an ultimate strength of ≈ 494 MPa, a yield strength of ≈ 260 MPa, and a fracture strain of ≈ 10.24%. The annealing lead to an increase in ductility, while practically maintaining its yield and ultimate strength. Overall, both samples have potential to be applied in structural applications.

In the future, additional tests can be made to complement the existent research. Namely, fatigue testing, an important test for structural materials because it determines the lifespan when subjected to cyclic loading. Another possible mechanical test is compressive testing to determine the material ability to withstand axial compression. For a more in-depth understanding of the microstructure and the present phases thermodynamics calculations, Scheil calculations could be made, since they are useful for predicting the solidification behavior as well as phase composition.

BIBLIOGRAPHY

[1] N. Shah, D. M J, R. M R, and G. Phanikumar, "Microstructure prediction of eutectic high entropy alloy using physical and computer simulation for additive manufacturing condition," *J. Alloys Compd.*, vol. 929, p. 167268, Dec. 2022. https://doi.org/10.1016/j.jallcom.2022.167268

[2] S. Park, H. Nam, J. Park, Y. Na, H. Kim, and N. Kang, "Superior-tensile property of CoCrFeMnNi alloys achieved using friction-stir welding for cryogenic applications," *Mater. Sci. Eng. A*, vol. 788, no. March, p. 139547, 2020. https://doi.org/10.1016/j.msea.2020.139547

[3] Z. Wu, S. A. David, Z. Feng, and H. Bei, "Weldability of a high entropy CrMnFeCoNi alloy," *Scr. Mater.*, vol. 124, pp. 81–85, 2016. https://doi.org/10.1016/j.scriptamat.2016.06.046

[4] L. H. Shah and M. Ishak, "Review of research progress on aluminum-steel dissimilar welding," *Mater. Manuf. Process.*, vol. 29, no. 8, pp. 928–933, 2014. http://dx.doi.org/10.1080/10426914.2014.880461

[5] J. W. Yeh *et al.*, "Nanostructured high-entropy alloys with multiple principal elements: Novel alloy design concepts and outcomes," *Adv. Eng. Mater.*, vol. 6, no. 5, pp. 299–303, 2004. https://doi.org/10.1002/adem.200300567

[6] J. Guo *et al.*, "Welding of high entropy alloys-A review," *Entropy*, vol. 21, no. 4, pp. 1–17, 2019. https://doi.org/10.3390/e21040431

[7] B. Gludovatz, A. Hohenwarter, D. Catoor, E. H. Chang, E. P. George, and R. O. Ritchie, "A fracture-resistant high-entropy alloy for cryogenic applications," *Science (80-.).*, vol. 345, no. 6201, pp. 1153–1158, 2014. https://doi.org/10.1126/science.1254581

[8] C. P. Lee, Y. Y. Chen, C. Y. Hsu, J. W. Yeh, and H. C. Shih, "The Effect of Boron on the Corrosion Resistance of the High Entropy Alloys Al[sub 0.5]CoCrCuFeNiB[sub x]," *J. Electrochem. Soc.*, vol. 154, no. 8, p. C424, 2007. http://dx.doi.org/10.1149/1.2744133

[9] M. H. Tsai and J. W. Yeh, "High-entropy alloys: A critical review," *Mater. Res. Lett.*, vol. 2, no. 3, pp. 107–123, 2014. https://doi.org/10.1080/21663831.2014.912690

[10] B. Cantor, I. T. H. Chang, P. Knight, and A. J. B. Vincent, "Microstructural development in equiatomic multicomponent alloys," *Mater. Sci. Eng. A*, vol. 375–377, no. 1-2 SPEC. ISS., pp. 213–218, 2004. https://doi.org/10.1016/j.msea.2003.10.257

[11] F. Otto, Y. Yang, H. Bei, and E. P. George, "Relative effects of enthalpy and entropy on the phase stability of equiatomic high-entropy alloys," *Acta Mater.*, vol. 61, no. 7, pp. 2628–2638, 2013. https://doi.org/10.1016/j.actamat.2013.01.042

[12] M. J. Yao, K. G. Pradeep, C. C. Tasan, and D. Raabe, "A novel, single phase, non-equiatomic FeMnNiCoCr high-entropy alloy with exceptional phase stability and tensile ductility," *Scr. Mater.*, vol. 72–73, pp. 5–8, 2014. https://doi.org/10.1016/j.scriptamat.2013.09.030

[13] K. Y. Tsai, M. H. Tsai, and J. W. Yeh, "Sluggish diffusion in Co-Cr-Fe-Mn-Ni high-entropy alloys," *Acta Mater.*, vol. 61, no. 13, pp. 4887–4897, 2013. https://doi.org/10.1016/j.actamat.2013.04.058

[14] A. V. Korchuganov and I. S. Lutsenko, "Molecular dynamics research of mechanical, diffusion

and thermal properties of CoCrFeMnNi high-entropy alloys," *AIP Conf. Proc.*, vol. 2053, 2018. https://doi.org/10.1063/1.5084484
[15] Z. Wang *et al.*, "Growth, microstructure and mechanical properties of CoCrFeMnNi high entropy alloy films," *Vacuum*, vol. 179, no. March, p. 109553, 2020. https://doi.org/10.1016/j.vacuum.2020.109553
[16] C. Dang, J. U. Surjadi, L. Gao, and Y. Lu, "Mechanical properties of nanostructured CoCrFeNiMn high-entropy alloy (HEA) coating," *Front. Mater.*, vol. 5, no. August, pp. 1–6, 2018. https://doi.org/10.3389/fmats.2018.00041
[17] J. P. Oliveira *et al.*, "Gas tungsten arc welding of as-rolled CrMnFeCoNi high entropy alloy," *Mater. Des.*, vol. 189, p. 108505, 2020. https://doi.org/10.1016/j.matdes.2020.108505
[18] D. Pandya, A. Badgujar, and N. Ghetiya, "A novel perception toward welding of stainless steel by activated TIG welding: a review," *Mater. Manuf. Process.*, vol. 36, no. 8, pp. 877–903, 2021. https://doi.org/10.1080/10426914.2020.1854467
[19] M. Kurtulmus, "Activated flux TIG welding of austenitic stainless steels," *Emerg. Mater. Res.*, vol. 9, no. 4, pp. 1041–1055, 2020. https://doi.org/10.1680/jemmr.18.00092
[20] N. Solomon and I. Solomon, "Effect of deformation-induced phase transformation on AISI 316 stainless steel corrosion resistance," *Eng. Fail. Anal.*, vol. 79, pp. 865–875, 2017. https://doi.org/10.1016/j.engfailanal.2017.05.031
[21] H. Y. Huang, S. W. Shyu, K. H. Tseng, and C. P. Chou, "Evaluation of TIG flux welding on the characteristics of stainless steel," *Sci. Technol. Weld. Join.*, vol. 10, no. 5, pp. 566–573, 2005. https://doi.org/10.1179/174329305X48329
[22] J. P. Oliveira, B. Crispim, Z. Zeng, T. Omori, F. M. Braz Fernandes, and R. M. Miranda, "Microstructure and mechanical properties of gas tungsten arc welded Cu-Al-Mn shape memory alloy rods," *J. Mater. Process. Technol.*, vol. 271, no. December 2018, pp. 93–100, 2019. https://doi.org/10.1016/j.jmatprotec.2019.03.020
[23] A. V. Adedayo, S. A. Ibitoye, and O. A. Oyetoyan, "Annealing Heat Treatment Effects on Steel Welds," *J. Miner. Mater. Charact. Eng.*, vol. 09, no. 06, pp. 547–557, 2010. http://dx.doi.org/10.4236/jmmce.2010.96039
[24] C. W. Tsai, Y. L. Chen, M. H. Tsai, J. W. Yeh, T. T. Shun, and S. K. Chen, "Deformation and annealing behaviors of high-entropy alloy Al0.5CoCrCuFeNi," *J. Alloys Compd.*, vol. 486, no. 1–2, pp. 427–435, 2009. https://doi.org/10.1016/j.jallcom.2009.06.182
[25] P. P. Bhattacharjee *et al.*, "Microstructure and texture evolution during annealing of equiatomic CoCrFeMnNi high-entropy alloy," *J. Alloys Compd.*, vol. 587, pp. 544–552, 2014. https://doi.org/10.1016/j.jallcom.2013.10.237
[26] N. Kashaev, V. Ventzke, N. Stepanov, D. Shaysultanov, V. Sanin, and S. Zherebtsov, "Laser beam welding of a CoCrFeNiMn-type high entropy alloy produced by self-propagating high-temperature synthesis," *Intermetallics*, vol. 96, no. December 2017, pp. 63–71, 2018. https://doi.org/10.1016/j.intermet.2018.02.014
[27] J. P. Oliveira *et al.*, "Dissimilar laser welding of a CoCrFeMnNi high entropy alloy to 316 stainless steel," *Scr. Mater.*, vol. 206, p. 114219, 2022. https://doi.org/10.1016/j.scriptamat.2021.114219
[28] K. Zhang and Z. Fu, "Effects of annealing treatment on phase composition and microstructure of CoCrFeNiTiAl x high-entropy alloys," *Intermetallics*, vol. 22, pp. 24–32, 2012. https://doi.org/10.1016/j.intermet.2011.10.010
[29] T. Sourmail, P. Opdenacker, G. Hopkin, and H. K. D. H. Bhadeshia, "Metals and Alloys Annealing Twins," *Univ. Cambridge-shows twin boundarys*, pp. 1–7, 2014.
[30] Z. Peng, Z. Fan, M. R. Abdullah, C. Ren, J. Li, and P. Gong, "Corrosion Resistance Enhancement of CoCrFeMnNi High-Entropy Alloy with WC Particle Reinforcements via Laser Melting Deposition," *Materials (Basel).*, vol. 16, no. 13, p. 4701, 2023. https://doi.org/10.3390/ma16134701
[31] M. Dadfar, M. H. Fathi, F. Karimzadeh, M. R. Dadfar, and A. Saatchi, "Effect of TIG welding on corrosion behavior of 316L stainless steel," *Mater. Lett.*, vol. 61, no. 11–12, pp. 2343–2346, 2007. https://doi.org/10.1016/j.matlet.2006.09.008

[32] A. E. Karantzalis, A. Poulia, S. Kamnis, A. Sfikas, A. Fotsis, and E. Georgatis, "Modification of Cantor High Entropy Alloy by the Addition of Mo and Nb: Microstructure Evaluation, Nanoindentation-Based Mechanical Properties, and Sliding Wear Response Assessment," *Alloys*, vol. 1, no. 1, pp. 70–92, 2022. https://doi.org/10.3390/alloys1010006

[33] Z. Zeng *et al.*, "Mechanical properties of Cantor alloys driven by additional elements: a review," *J. Mater. Res. Technol.*, vol. 15, pp. 1920–1934, 2021. https://doi.org/10.1016/j.jmrt.2021.09.019

[34] K. Wang, D. Wang, and F. Han, "Effect of crystalline grain structures on the mechanical properties of twinning-induced plasticity steel," *Acta Mech. Sin. Xuebao*, vol. 32, no. 1, pp. 181–187, 2016. https://doi.org/10.1007/s10409-015-0513-7

[35] M. Vilémová *et al.*, "Thermal and Oxidation Behavior of CoCrFeMnNi Alloy with and Without Yttrium Oxide Particle Dispersion," *J. Mater. Eng. Perform.*, vol. 28, no. 9, pp. 5850–5859, 2019. https://doi.org/10.1007/s11665-019-04311-9

[36] P. Das, S. Bathula, and S. Gollapudi, "Evaluating the effect of grain size distribution on thermal conductivity of thermoelectric materials," *Nano Express*, vol. 1, no. 2, 2020. https://doi.org/10.1088/2632-959X/abb43f

[37] F. Otto, N. L. Hanold, and E. P. George, "Microstructural evolution after thermomechanical processing in an equiatomic, single-phase CoCrFeMnNi high-entropy alloy with special focus on twin boundaries," *Intermetallics*, vol. 54, pp. 39–48, 2014. https://doi.org/10.1016/j.intermet.2014.05.014

[38] *ASM Handbook*, 10th ed., vol. 1. ASM International, 1990.

[39] T. N. Lam *et al.*, "Tensile Response of As-Cast CoCrFeNi and CoCrFeMnNi High-Entropy Alloys," *Crystals*, vol. 12, no. 2, 2022. https://doi.org/10.3390/cryst12020157

2023 MARTIM MESTRE DISSIMILAR WELDING OF CoCrFeMnNi HIGH ENTROPY ALLOY TO 316 STAINLESS STEEL

NOVA SCHOOL OF SCIENCE & TECHNOLOGY